Possibilities for the synthesis of superheavy element Z = 121 in fusion reactions*

Ming-Hao Zhang,[1,2] Yu-Hai Zhang,[1,2] Ying Zou,[1,2] Xiu-Xiu Yang,[1,2] Gen Zhang,[3] and Feng-Shou Zhang[1,2,4,†]

[1] *The Key Laboratory of Beam Technology of Ministry of Education, College of Nuclear Science and Technology, Beijing Normal University, Beijing 100875, China*

[2] *Institute of Radiation Technology, Beijing Academy of Science and Technology, Beijing 100875, China*

[3] *School of Physical Science and Technology, Guangxi University, Nanning 530004, China*

[4] *Center of Theoretical Nuclear Physics, National Laboratory of Heavy Ion Accelerator of Lanzhou, Lanzhou 730000, China*

Based on the dinuclear system model, the calculated evaporation residue cross sections match well with the current experimental results. we systematically study the synthesis of superheavy element $Z = 121$ through combinations of stable projectiles with $Z = 21-30$ and targets with half-lives exceeding 50 days. The influence of mass asymmetry and the isotopic dependence of projectile and target nuclei are investigated in detail. The reactions ^{254}Es (^{46}Ti, 3n) ^{297}121 and ^{252}Es (^{46}Ti, 3n) ^{295}121 are found to be experimentally feasible for synthesizing superheavy element $Z = 121$, with the maximal evaporation residue cross sections of 6.619 fb at 219.9 MeV and 4.123 fb at 223.9 MeV.

Keywords: Superheavy nuclei, Dinuclear system model, Fusion reaction, Evaporation residue cross section

I. INTRODUCTION

The production of new superheavy nuclei (SHN) represents a challenging frontier in the realm of low-energy nuclear reaction. Over the years, experimental and theoretical nuclear physicists have explored SHN synthesis since the prediction of the "island of stability" around Z = 114, N = 184 [1, 2], and the Skyrme-Hartree-Fock method considers Z = 120, 124 or 126 and N = 172 or 184 as magic numbers [3]. The synthesis of superheavy elements (SHEs) Z = 107-112 was accomplished in GSI using cold fusion reactions with Pb and Bi targets [4]. However, despite the successful synthesis of SHE $Z = 113$ via cold fusion reaction ^{70}Zn + ^{209}Bi at RIKEN [5], the evaporation residue cross section (ERCS) $\sigma_{\rm ER}$ was only 0.03 pb, reaching the limit of experimental detection at that time [6]. To overcome this challenge, researchers in Dubna turned to hot fusion reactions with ^{48}Ca beams and actinide targets. This method results in the production of SHEs Z = 114-118 [7–12], which completes the seventh period of the periodic table.

In recent years, many new isotopes with $Z \leq 118$ were synthesized using modern accelerators, such as DC-280 and U-400 of Dubna SHE factory, RILAC of RIKEN, SFC of HIRFL and UNILAC of GSI [7, 12–16], but the production of SHEs $Z > 118$ remains a challenge. Previous attempts to produce SHE $Z = 120$ using ^{58}Fe+^{244}Pu [6] and ^{54}Cr + ^{248}Cm [17] reactions at Dubna and GSI, respectively, did not observe any α decay chains associated with this element. The three events reported by GSI in Ref. [17] were later found to be random events [18]. In 2020, with the gas-filled recoil separator TASCA at GSI, search for synthesizing the SHEs $Z = 119$ and $Z = 120$ was conducted via the reactions ^{50}Ti + ^{249}Bk and ^{50}Ti + ^{249}Cf, yet neither was detected [19]. In 2022, RIKEN estimated the optimal incident energy for synthesizing SHE $Z = 119$ through the reaction ^{51}V+^{248}Cm [20]. Therefore, the synthesis of SHEs $Z > 118$ requires not only more advanced detection and identification techniques, but also an appropriate reaction system.

In order to describe the process of fusion-evaporation reactions accurately, several models and different fusion mechanisms were proposed. The improved quantum molecular dynamics (ImQMD) model [21], time-dependent Hartree-Fock theory [22–25], fusion-by-diffusion model [26], cluster dynamical decay model [27], two-step model [28, 29], dinuclear system (DNS) model [30–44] and other methods [45–48] are proved to be reliable in reproducing experimental data and also have given predictions about the synthesis of unknown nuclei [22, 45, 49–56].

The synthesis and decay of elements $Z = 119$ and $Z = 120$ has been extensively studied theoretically [22, 33, 35, 45, 52, 57–59], whereas only a limited number of calculations have been conducted on the synthesis of SHE $Z = 121$. To address this research gap, this paper aims to investigate the optimal projectile-target combinations to synthesize SHE $Z = 121$ and provide a reference for future experimental attempts.

The paper is organized as follows. In sect. II, we describe the DNS model and examine the predicting reliability. The ERCSs of $Z = 121$ isotopes in different reaction channels are discussed in sect. III. Finally, we make a conclusion in sect. IV.

II. THEORETICAL DESCRIPTIONS

In the DNS model, the ERCS of synthesizing SHN in the center of-mass frame can be obtained with the following expression:

$$\sigma_{\rm ER}(E_{\rm c.m.}) = \frac{\pi\hbar^2}{2\mu E_{\rm c.m.}} \sum_J (2J+1)T(E_{\rm c.m.},J) \times P_{\rm CN}(E_{\rm c.m.},J)W_{\rm sur}(E_{\rm c.m.},J). \tag{1}$$

Here $T\left(E_{\rm c.m.}, J\right)$ represents the transmission probability for colliding system to overcome the Coulomb barrier $V_{\rm b}$.

* Supported by the National Key R&D Program of China under Grant No. 2023YFA1606401 and the National Natural Science Foundation of China under Grants No.12135004, No.11635003 and No.11961141004.

† Corresponding author, fszhang@bnu.edu.cn

$P_{\rm CN}\left(E_{\rm c.m.},J\right)$ is the fusion probability for forming a compound nucleus [60]. $W_{\rm sur}\left(E_{\rm c.m.},J\right)$ denotes the survival probability that the excited compound nucleus emits neutron, instead of undergoing fission, to reach the ground state [61]. The nucleus-nucleus interaction potential considering the quadrupole deformation is expressed as following [62]:

$$\begin{aligned}V(R,\beta_1,\beta_2,\theta_1,\theta_2) = {} & \frac{1}{2}C_1(\beta_1-\beta_1^0)^2+\frac{1}{2}C_2(\beta_2-\beta_2^0)^2\\ & +V_{\rm C}(R,\beta_1,\beta_2,\theta_1,\theta_2)\\ & +V_{\rm N}(R,\beta_1,\beta_2,\theta_1,\theta_2).\end{aligned} \tag{2}$$

In this formula, $\beta_{1,2}$ and $\beta_{1,2}^0$ denote the dynamical quadrupole deformation parameters and static deformation parameters for projectile and target nucleus, respectively. $\theta_{1,2}$ are the collision angles for deformed projectile and target nucleus, respectively. The stiffness parameters $C_{1,2}$ is written as [63]:

$$C_i=(\lambda-1)\left[(\lambda+2)R_{0,i}^2\sigma-\frac{3}{2\pi}\frac{Z_i^2e^2}{R_{0,i}(2\lambda+1)}\right]. \tag{3}$$

$\lambda=2$ represents the quadrupole deformation. The Coulomb potential $V_{\rm C}$ is determined using Wang formula [64]:

$$\begin{aligned}V_{\rm C}(R,\beta_1,\beta_2,\theta_1,\theta_2) = {} & \frac{Z_1Z_2e^2}{R}+\sqrt{\frac{9}{20\pi}}\frac{Z_1Z_2e^2}{R^3}\\ & \times\sum_{i=1,2}R_i^2\beta_2^{(i)}P_2(\cos\theta_i)+\frac{3}{7\pi}\\ & \times\frac{Z_1Z_2e^2}{R^3}\sum_{i=1,2}R_i^2[\beta_2^{(i)}P_2(\cos\theta_i)]^2.\end{aligned} \tag{4}$$

The nuclear potential $V_{\rm N}$ is given by the Woods-Saxon potential [64]:

$$\begin{aligned}&V_{\rm N}(R,\beta_1,\beta_2,\theta_1,\theta_2)=-V_0\times\\ &\left\{1+\exp\left[\frac{r-\sum_{i=1,2}R_i\left(1+\sqrt{5/4\pi}\beta_2^{(i)}P_2(\cos\theta_i)\right)}{a}\right]\right\}\end{aligned} \tag{5}$$

In the capture process, the transmission probability $T(E_{\rm c.m.},B,J)$ is described via the Ahmed formula [65, 66]:

$$T(E_{\rm c.m.},B,J)=\frac{1-\exp(-4\pi\alpha)}{1+\exp(2\pi(\beta_J-\alpha))}. \tag{6}$$

Here $\alpha=\frac{\sqrt{2\mu E_{\rm c.m.}}}{\hbar}\alpha_{\rm M}$ and $\beta_J=\frac{\sqrt{2\mu\left(B+\frac{\hbar^2}{2\mu R_{\rm B}^2(J)}J(J+1)\right)}}{\hbar}\alpha_{\rm M}$. μ represents the reduced mass and $\alpha_{\rm M}$ denotes the Morse parameter [67].

Taking into account the barrier distribution function $f\left(B\right)$, $T\left(E_{\rm c.m.},J\right)$ is written as:

$$T\left(E_{\rm c.m.},J\right)=\int f\left(B\right)T\left(E_{\rm c.m.},B,J\right)dB. \tag{7}$$

The asymmetric barrier distribution parameters are given in Ref. [68]. The capture cross section $\sigma_{\rm cap}$ is calculated as follows [62]:

$$\sigma_{\rm cap}\left(E_{\rm c.m.}\right)=\frac{\pi\hbar^2}{2\mu E_{\rm c.m.}}\sum_J\left(2J+1\right)T\left(E_{\rm c.m.},J\right). \tag{8}$$

The fusion of the colliding nuclei is determined by the potential energy surface expressed as [62]:

$$\begin{aligned}&U\left(N_1,Z_1,N_2,Z_2,R,\beta_1,\beta_2\right)\\ &=E_{\rm B}\left(N_1,Z_1\right)+E_{\rm B}\left(N_2,Z_2\right)-E_{\rm B}\left(N_3,Z_3\right)\\ &\quad+V_{\rm CN}\left(N_1,Z_1,N_2,Z_2,R,\beta_1,\beta_2\right).\end{aligned} \tag{9}$$

The data of the binding energies of the colliding nucleus $E_{\rm B}\left(N_{1,2},Z_{1,2}\right)$ and the formed compound nucleus $E_{\rm B}\left(N_3,Z_3\right)$ is taken from Ref. [69]. $V_{\rm CN}$ denotes the nucleus-nucleus interaction potential.

The nucleon transfer is treated as a diffusion process at the lowest point of the potential energy surface, known as the driving potential [62]. To form a compound nucleus, the dinuclear system must surpass the inner fusion barrier $B_{\rm fus}$ along the mass asymmetry degree $\eta=\left(A_P-A_T\right)/\left(A_P+A_T\right)$, which denotes the potential energy disparity between the incident point and the Businaro-Gallone (B.G.) point (the peak of the driving potential) [70], defined as $B_{\rm fus}=U\left(\eta_{\rm B.G.}\right)-U\left(\eta_{\rm i}\right)$. The fusion probability $P_{\rm CN}(E_{\rm c.m.},J)$ is determined through the summation of the distribution probabilities of crossing the B.G. point $P\left(N_1,Z_1,E_1,t\right)$ as follows:

$$P_{\rm CN}(E_{\rm c.m.},J)=\sum_{N_1=1}^{N_{\rm B.G.}}\sum_{Z_1=1}^{Z_{\rm B.G.}}P(N_1,Z_1,E_1,t=\tau_{\rm int}(J)). \tag{10}$$

Here the interaction time $\tau_{\rm int}(J)$ is calculated via the deflection function method [71]. $P\left(N_1,Z_1,E_1,t\right)$ is calculated through solving the two-dimensional master equation:

$$\begin{aligned}&\frac{dP(N_1,Z_1,E_1,t)}{dt}\\ &=\sum_{N_1'}W_{N_1,Z_1;N_1',Z_1}(t)\\ &\quad\times[d_{N_1,Z_1}P(N_1',Z_1,E_1,t)-d_{N_1',Z_1}P(N_1,Z_1,E_1,t)]\\ &+\sum_{Z_1'}W_{N_1,Z_1;N_1,Z_1'}(t)\\ &\quad\times[d_{N_1,Z_1}P(N_1,Z_1',E_1,t)-d_{N_1,Z_1'}P(N_1,Z_1,E_1,t)]\\ &-[\Lambda_{\rm qf}(\Theta(t))+\Lambda_{\rm fis}\left(\Theta(t)\right)]P(N_1,Z_1,E_1,t).\end{aligned} \tag{11}$$

Here $W_{N_1,Z_1;N_1',Z_1}$ denotes the mean transition probability from state $\left(N_1,Z_1\right)$ to state $\left(N_1',Z_1\right)$ [72], d_{N_1,Z_1} is the microscopic dimension of state $\left(N_1,Z_1\right)$. The quasi-fission rate

$\Lambda_{\rm qf}$ and fission rate $\Lambda_{\rm fis}$ can be given by the one-dimensional Kramers formula [73].

The survival process is primarily determined by the rivalry between fission and neutron emission [74]. The survival probability at the excitation energy $E^*_{\rm CN}$ can be expressed as:

$$W_{\rm sur}(E^*_{\rm CN}, x, J) = P(E^*_{\rm CN}, x, J) \prod_{i=1}^{x} \left[\frac{\Gamma_{\rm n}(E^*_i, J)}{\Gamma_{\rm n}(E^*_i, J) + \Gamma_{\rm f}(E^*_i, J)}\right]. \quad (12)$$

$P\,(E^*_{\rm CN}, x, J)$ denotes the realization probability for emitting x neutrons [75]. E^*_i represents the excitation energy of the compound nucleus which have emitted $i-1$ neutrons [57].

The neutron decay width $\Gamma_{\rm n}(E^*_i, J)$ is calculated using the Weisskopf-Ewing theory [76]:

$$\Gamma_{\rm n}(E^*_i, J) = \frac{(2s_{\rm n}+1)m_{\rm n}}{\pi^2\hbar^2\rho(E^*_i, J)} \times \int_{I_{\rm n}} \varepsilon\rho(E^*_i - B_{\rm n} - \varepsilon, J)\sigma_{\rm inv}(\varepsilon)d\varepsilon. \quad (13)$$

Here $I_{\rm n} = \left[0, E^*_i - B_{\rm n} - \delta - \frac{1}{a}\right]$. δ and $B_{\rm n}$ represent the pairing correction and the the neutron separation energy [33], respectively. The level density ρ is expressed as in Ref. [77] and $\sigma_{\rm inv}$ denotes the inverse reaction cross section [78].

$\Gamma_{\rm f}(E^*_i, J)$ is the fission decay width given by Bohr-Wheeler transition-state method [79]:

$$\Gamma_{\rm f}(E^*_i, J) = \frac{1}{2\pi\rho_{\rm f}(E^*_i, J)} \times \int_{I_{\rm f}} \frac{\rho_{\rm f}(E^*_i - B_{\rm f}(E^*_i, J) - \varepsilon, J)d\varepsilon}{1 + \exp\left[-2\pi(E^*_i - B_{\rm f}(E^*_i, J) - \varepsilon)/\hbar\omega\right]}, \quad (14)$$

with $I_{\rm f} = \left[0, E^*_i - B_{\rm f}(E^*_i, J) - \delta - \frac{1}{a_{\rm f}}\right]$, $a_{\rm f} = 1.1A/12$ [80, 81]. The temperature-dependent fission barrier $B_{\rm f}(E^*_i, J)$ is calculated by the following expression [82, 83]:

$$B_{\rm f}(E^*_i, J) = B_{\rm f}^{\rm LD}(1 - x_{\rm LD}T_i^2) + B_{\rm f}^{\rm M}(E^*_i = 0, J)\exp\left(-\frac{E^*_i}{E_{\rm D}}\right) - \left(\frac{\hbar^2}{2J_{\rm g.s.}} - \frac{\hbar^2}{2J_{\rm s.d.}}\right)J(J+1). \quad (15)$$

Here ${B_{\rm f}}^{\rm LD}$ denotes the macroscopic part of the fission barrier. T_i and $x_{\rm LD}$ represent the nuclear temperature and the temperature dependent parameter, respectively [82]. ${B_{\rm f}}^{\rm M}$ is the microscopic shell correction energy in the ground state [69] and $E_{\rm D}$ = 25 MeV [50]. $J_{\rm g.s.}$ and $J_{\rm s.d.}$ are expressed as in Ref. [84, 85].

To evaluate the accuracy of employing our model for predicting the ERCSs of SHN, we present in Fig. 1 the comparisons between calculated ERCSs and the experimental data in the reactions ^{48}Ca + ^{245}Cm [12, 86], ^{48}Ca + ^{248}Cm [87], ^{48}Ca + ^{249}Bk [88] and ^{48}Ca + ^{249}Cf [12, 89, 90]. The calculation uncertainties arise from the relatively subjective choice of $E_{\rm D}$ range [91]. The fission barrier heavily relies on the contribution of the shell correction energy, and the reduction of the shell correction energy with increasing excitation energy is described by the $E_{\rm D}$ values, which lies in the range 10 MeV $\leq E_{\rm D} \leq$ 30 MeV [92].

As shown in Figs. 1(a)-(d), the ERCSs show a decreasing trend with increasing proton number of compound nucleus. For the reactions ^{48}Ca + ^{245}Cm and ^{48}Ca + ^{249}Cf, the maximal ERCSs of both calculation and experiment appear in the 3n-emission channels. The 4n-emission channels are more favorable for the synthesis of SHN with the reactions ^{48}Ca + ^{248}Cm and ^{48}Ca + ^{249}Bk. The predicted ERCSs align well with the experimental results, especially for the reaction ^{48}Ca + ^{249}Cf. A maximal ERCS of $0.42^{+0.87}_{-0.30}$ pb for the reaction ^{48}Ca + ^{249}Cf is predicted at the 3n-emission channel at $E^*_{\rm CN}$ = 32.0 MeV, which is consistent with the experimental value of $0.5^{+1.6}_{-0.3}$ pb with $E^*_{\rm CN}$ = 32.1 − 36.6 MeV at the same channel. This validates the applicability of the DNS model in the prediction of synthesizing new elements via fusion-evaporation reactions.

III. RESULTS AND DISCUSSION

To avoid facility contamination by unstable beam, we choose stable projectiles with Z = 21 − 30 and actinide targets with half-lives exceeding 50 days for the experimental duration, and the optimal reaction systems are summarized in Table 1. One can see that the most favorable reactions and ERCSs (the optimal $E_{\rm c.m.}$) for producing isotopes $^{295-302}$121 are ^{252}Es (^{46}Ti, 3n) ^{295}121, 4.123 fb (223.9 MeV), ^{248}Cf (^{50}V, 3n) ^{296}121, 0.566 fb (239.1 MeV), ^{254}Es (^{46}Ti, 3n) ^{297}121, 6.619 fb (219.9 MeV), ^{254}Es (^{47}Ti, 3n) ^{298}121, 1.331 fb (222.3 MeV), ^{257}Fm (^{45}Sc, 3n) ^{299}121, 8.778 fb (213.6 MeV), ^{254}Es (^{49}Ti, 3n) ^{300}121, 0.453 fb (228.5 MeV), ^{254}Cf (^{50}V, 3n) ^{301}121, 3.705 fb (229.0 MeV) and ^{254}Cf (^{51}V, 3n) ^{302}121, 0.524 fb (234.1 MeV).

As mentioned in the previous paragraph, the largest maximal ERCS corresponding to the synthesis of SHE with Z = 121 is 8.778 fb in the reaction ^{45}Sc+^{257}Fm. Besides, the reactions ^{46}Ti+^{252}Es and ^{46}Ti+^{254}Es offer large maximal ERCSs of 4.123 and 6.619 fb. Considering the experimental feasibility, The ^{254}Es target is currently available among several Es targets in laboratory [94], with a half-life of 275.70 d. The ^{252}Es target has a comparatively longer half-life of 1.29 y, making it a potential target for experimental purposes. Therefore, despite a slightly higher ERCS of the reaction ^{45}Sc+^{257}Fm, the reactions ^{46}Ti+^{252,254}Es are more feasible for experimental purposes.

In Figs. 2(a)-(c), we present the calculated ERCSs of the reactions ^{45}Sc+^{257}Fm, ^{48}Ti+^{254}Es and ^{51}V+^{251}Cf. These reactions yield the same compound nuclei of ^{302}121. Notably, our analysis reveals a consistent diminishing trend in the maximal ERCSs for synthesizing the same isotopes, ^{299}121 via the 3n-emission channel and ^{298}121 via the 4n-emission channel, as the charge number of the projectiles increases. This trend can

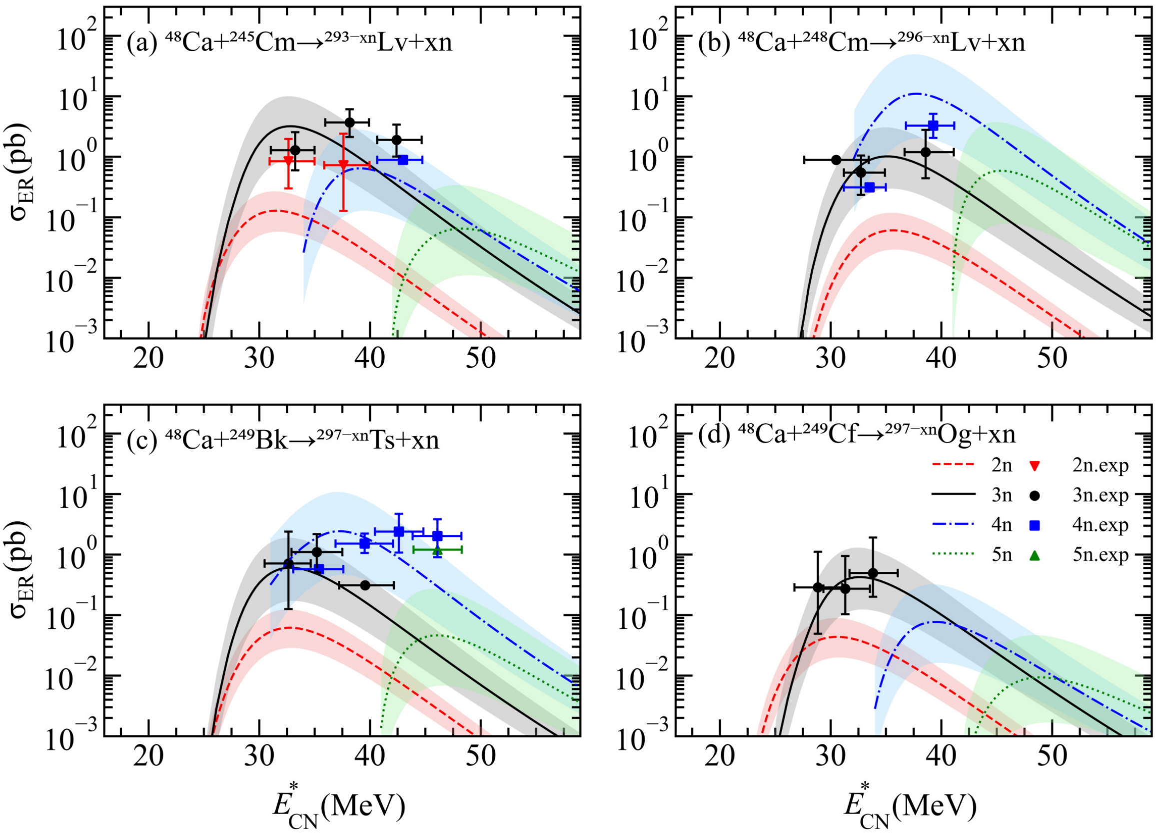

Fig. 1. (Color online) Comparison of the predicted ERCSs with the experimental results [12, 86–90] for the synthesis of Lv (a, b), Ts (c), and Og (d). The calculated ERCSs in the 2n, 3n, 4n and 5n-emission channels are denoted by the dashed, solid, dash-dot and dotted lines, respectively. The shades indicate the uncertainties of calculated ERCSs. The experimental results for the 2n, 3n, 4n, and 5n-emission channels are denoted by inverted triangles, circles, squares and triangles, respectively.

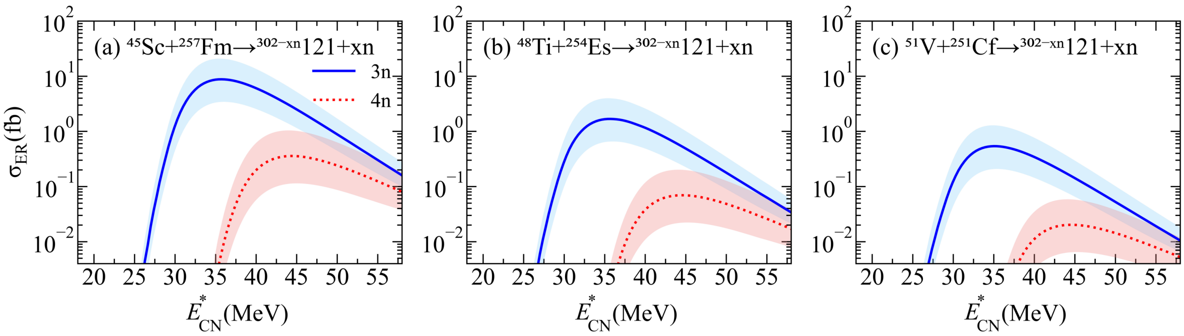

Fig. 2. (Color online) The predicted ERCSs of the reactions ^{45}Sc$+^{257}$Fm, ^{48}Ti$+^{254}$Es and ^{51}V$+^{251}$Cf. The 3n and 4n-emission channels are indicated by the blue solid and red dotted lines, respectively. The shades indicate the uncertainties of calculated ERCSs.

be attributed to the reduced fusion probability resulting from the increased mass asymmetry. To further investigate the influence of mass asymmetry on the fusion-evaporation reaction, the fusion probabilities and the driving potential for the reactions ^{45}Sc+^{257}Fm, ^{48}Ti+^{254}Es and ^{51}V+^{251}Cf are presented in Fig. 3 and Fig. 4.

Fig. 3 reveals an ascending trend of the fusion probabilities with the increasing E^*_{CN}. This occurs due to the heightened dissipated energy within the dinuclear system at higher E^*_{CN}, thus rendering the reaction system more likely to overcome the inner fusion barrier. Besides, it can be observed in Fig. 3 that the reaction ^{45}Sc+^{257}Fm exhibits much larger fusion probability compared to the other two reactions. Conversely, the fusion probability of the reaction ^{51}V+^{251}Cf is the lowest. This significant difference can be attributed to the different B_{fus} values influenced by the changed mass asymmetry.

Fig. 4 reveals that as the mass asymmetry of the reac-

TABLE 1. The favorable reaction systems for producing SHEs $Z = 121$. The isotopes, the reaction systems and the half-lives of corresponding targets [93] are presented in columns 1-3. The optimal incident energies $E_{\mathrm{c.m.}}$ and the E^*_{CN} are listed in columns 4-5, respectively. The maximal calculated ERCSs for certain neutron emission channel are shown in the columns 6.

Isotope	Reaction	$T_{1/2}$ (target)	$E_{\mathrm{c.m.}}$ (MeV)	E^*_{CN} (MeV)	σ_{ER} (fb)
$^{295}121$	^{252}Es(^{46}Ti,3n)	1.29 yr	223.9	36.0	$4.123^{+5.52}_{-2.495}$
$^{296}121$	^{248}Cf(^{50}V,3n)	333.50 d	239.1	36.0	$0.566^{+0.758}_{-0.342}$
$^{297}121$	^{254}Es(^{46}Ti,3n)	275.70 d	219.9	35.0	$6.619^{+9.196}_{-4.073}$
	^{249}Cf(^{51}V,3n)	351.00 yr	240.3	35.0	$0.306^{+0.426}_{-0.188}$
$^{298}121$	^{254}Es(^{47}Ti,3n)	275.70 d	222.3	36.0	$1.331^{+1.827}_{-0.813}$
$^{299}121$	^{257}Fm(^{45}Sc,3n)	100.50 d	213.6	36.0	$8.778^{+11.923}_{-5.339}$
	^{254}Es(^{48}Ti,3n)	275.70 d	227.6	36.0	$1.677^{+2.293}_{-1.02}$
	^{252}Cf(^{50}V,3n)	2.64 yr	232.3	34.0	$1.368^{+1.936}_{-0.842}$
	^{251}Cf(^{51}V,3n)	898.00 yr	238.2	35.0	$0.540^{+0.748}_{-0.332}$
$^{300}121$	^{254}Es(^{49}Ti,3n)	275.70 d	228.5	36.0	$0.453^{+0.594}_{-0.272}$
$^{301}121$	^{254}Cf(^{50}V,3n)	60.50 d	229.0	33.0	$3.705^{+4.912}_{-2.249}$
	^{254}Es(^{50}Ti,3n)	275.70 d	232.5	35.0	$0.541^{+0.688}_{-0.321}$
$^{302}121$	^{254}Cf(^{51}V,3n)	60.50 d	234.1	34.0	$0.524^{+0.636}_{-0.306}$

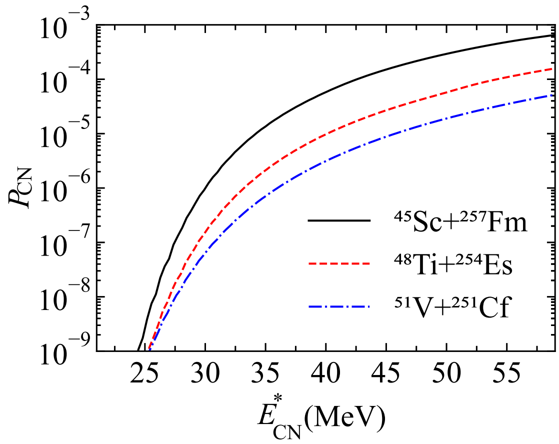

Fig. 3. (Color online) The calculated fusion probabilities of the reactions ^{45}Sc+^{257}Fm (black solid line), ^{48}Ti+^{254}Es (red dashed line) and ^{51}V+^{251}Cf (blue dash-dot line).

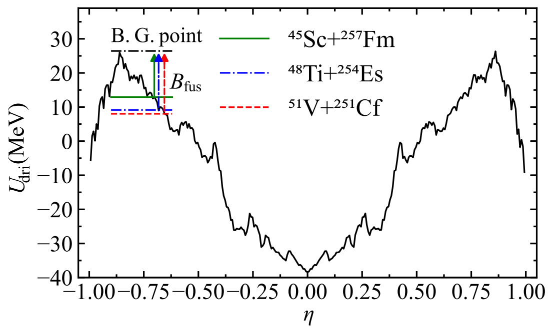

Fig. 4. (Color online) The driving potential for the reaction ^{45}Sc+^{257}Fm, ^{48}Ti+^{254}Es and ^{51}V+^{251}Cf as a function of mass asymmetry. The arrows indicate the entrance channel.

tion system decreases, the entrance channel approaches closer to the B.G. point, resulting in a corresponding decrease in the B_{fus} value. For the reaction ^{45}Sc+^{257}Fm, the B_{fus} is 13.1 MeV, which is lower than the reactions ^{48}Ti+^{254}Es (B_{fus}=17.1 MeV) and ^{51}V+^{251}Cf (B_{fus}=17.8 MeV). Consequently, the reaction ^{45}Sc+^{257}Fm is more likely to overcome the inner fusion barrier, resulting in an enhanced fusion probability in Fig. 3. Evidently, the heightened fusion probabilities, stemming from the reduced mass asymmetry, establishes the superiority of Sc and Ti-induced reactions for producing SHE with Z = 121.

In Fig. 5, we present an analysis of the calculated maximal ERCSs, the corresponding incident energies and Q values on the reactions involving $^{46-50}$Ti projectiles and ^{252,254}Es targets. Fig. 5(a) reveals that the reactions employing the neutron-rich ^{254}Es target consistently yield larger maximal ERCSs compared to those employing the ^{252}Es target. Moreover, the maximal ERCSs decrease as the neutron number of the projectiles increases. Notably, the odd-even effects also have an impact on the maximal ERCSs, with even-A Ti projectiles resulting in relatively enhanced ERCSs. Fig. 5(b) illustrates that the optimal incident energies for reactions with ^{252}Es target are about 3-4 MeV higher than those with ^{254}Es target. Additionally, the optimal incident energies exhibit a discernible increase with evident odd-even effects as the neutron number of the projectiles increases.

For all the reactions $^{46-50}$Ti+^{252}Es and $^{46-50}$Ti+^{254}Es, the corresponding E^*_{CN} fall within the range of 35-37 MeV. This range has a limited impact on the optimal incident energies. The increasing trend in optimal incident energies can be attributed to the differences in the Q values. Fig. 5(c) reveals that a high neutron excess of the target nuclei enhances the Q values of the reaction system, while a high neutron excess of the projectile nuclei exerts the opposite influence. The odd-even effects of the projectiles also have a significant influence on the Q values, with reactions utilizing the even-A Ti projectiles displaying relatively suppressed Q values compared

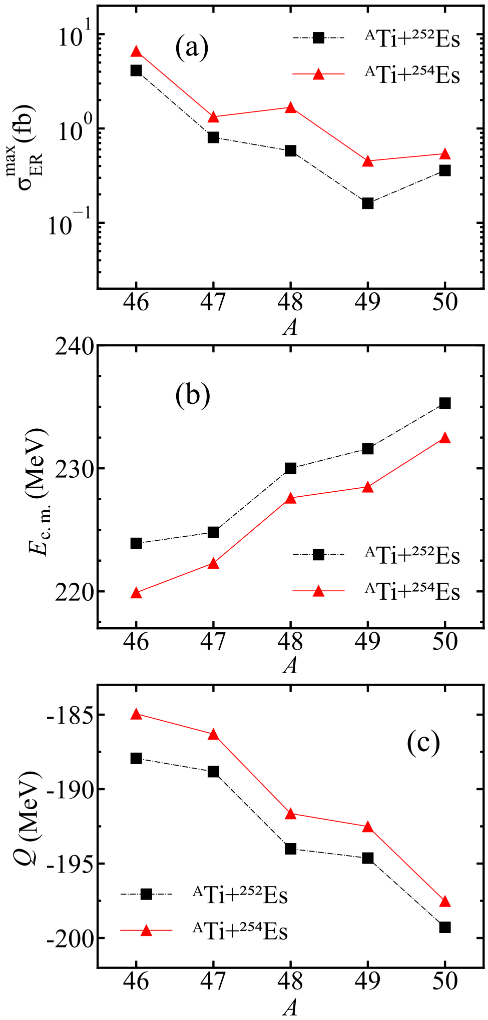

Fig. 5. (Color online) (a) The calculated maximal ERCSs, (b) the corresponding optimal incident energies and (c) the Q values of the reactions $^{46-50}$Ti+^{252}Es and $^{46-50}$Ti+^{254}Es.

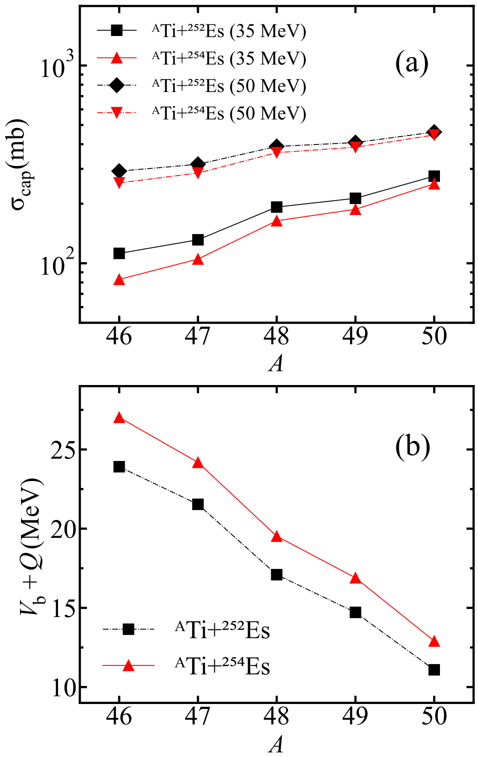

Fig. 6. (Color online) (a) The calculated capture cross sections of the reactions $^{46-50}$Ti+^{252}Es and $^{46-50}$Ti+^{254}Es with $E^*_{\rm CN}$ = 35 MeV and $E^*_{\rm CN}$ = 50 MeV. (b) The excitation energies of the corresponding Coulomb barriers $V_{\rm b} + Q$ of the reactions $^{46-50}$Ti+^{252}Es and $^{46-50}$Ti+^{254}Es.

to those employing the odd-A Ti projectiles.

To investigate the isotopic dependence on the maximal ERCSs and corresponding optimal incident energies, a comprehensive investigation of the capture, fusion, and survival stages is essential. In Fig. 6(a), we present the capture cross sections for the combinations involving $^{46-50}$Ti projectiles colliding with ^{252}Es and ^{254}Es targets at excitation energy of $E^*_{\rm CN}$ = 35 MeV and 50 MeV. Notably, the capture cross sections exhibit a rising trend with the increase of $E^*_{\rm CN}$, as the ability of surpassing the Coulomb barrier increases with higher $E^*_{\rm CN}$. Furthermore, it is evident that the capture cross sections of the reactions involving ^{252}Es targets are notably enhanced in comparison to those with ^{254}Es targets. Additionally, there is an upward trend in the capture cross sections with a higher neutron excess of the projectiles. These trend can be attributed to the decrease in the Coulomb barrier.

In Fig. 6(b) the excitation energies associated with the corresponding Coulomb barriers $V_{\rm b} + Q$ of the corresponding reactions are plotted. It can be observed that the $V_{\rm b} + Q$ values decreases with the rising neutron excess of the projectiles. Moreover, the reaction systems with the ^{252}Es target exhibit lower $V_{\rm b} + Q$ values compared to those with ^{254}Es target. Consequently, the reactions involving ^{252}Es as the target nuclei, coupled with neutron-rich Ti projectiles, have an increased likelihood of overcoming the Coulomb barrier, thereby enhancing the corresponding capture cross sections.

Regarding the fusion process, Fig. 7(a) shows the fusion probabilities of the reactions $^{46-50}$Ti+^{252}Es and $^{46-50}$Ti+^{254}Es at $E^*_{\rm CN}$ = 35 MeV and 50 MeV. As the increasing probabilities of overcoming the inner fusion barrier, the fusion probabilities are amplified with higher $E^*_{\rm CN}$. These fusion probabilities exhibit a decreasing trend with the increasing neutron excess of the projectiles. Notably, the employment of the neutron-rich ^{254}Es target leads to a relative enhancement of the fusion probability, which can be attributed to the reduced inner fusion barrier. In Fig. 7(b), the inner fusion barriers of the corresponding reactions are presented. It is evident that the $B_{\rm fus}$ values rise with the increasing neutron excess of the projectiles and are higher in the reaction systems with the lighter ^{252}Es target. This can be attributed to the increased mass asymmetry from the projectiles with higher neutron excess and targets with lower neutron excess, which subsequently enhances the $B_{\rm fus}$ values and

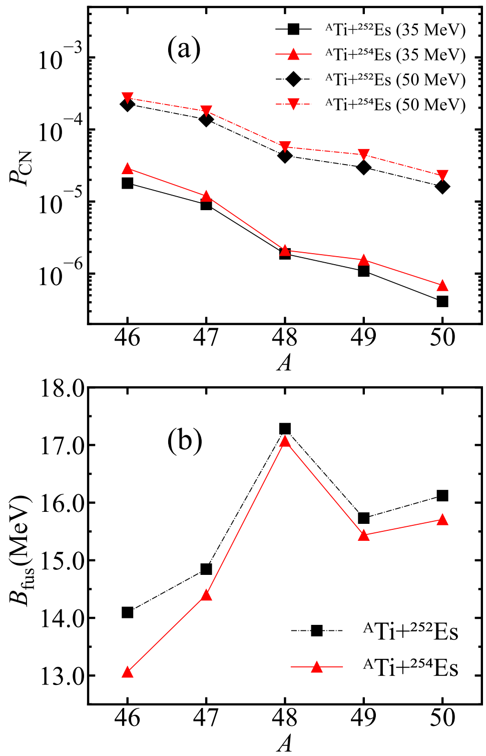

Fig. 7. (Color online) (a) The calculated fusion probabilities of the reactions $^{46-50}$Ti+^{252}Es and $^{46-50}$Ti+^{254}Es with $E^*_{\rm CN}$ = 35 MeV and $E^*_{\rm CN}$ = 50 MeV. (b) The $B_{\rm fus}$ values of the reactions $^{46-50}$Ti+^{252}Es and $^{46-50}$Ti+^{254}Es.

hinders the fusion process.

In Fig. 8(a), the survival probabilities of compound nuclei in the 3n-emission channel for the reactions $^{46-50}$Ti+^{252}Es and $^{46-50}$Ti+^{254}Es at $E^*_{\rm CN}$ = 35 MeV and 50 MeV are plotted. Notably, the survival probabilities exhibit a decreasing trend as the $E^*_{\rm CN}$ increases. This is due to the damped shell effect at increased $E^*_{\rm CN}$, resulting in diminished compound nucleus stability. Additionally, the ^{254}Es-based reactions exhibit relatively higher fusion probabilities with an obvious odd-even staggering pattern. This can be ascribed to the influence of the $B_{\rm n}$ and $B_{\rm f}$ values for the corresponding compound nuclei, as plotted in Fig. 8(b) and Fig. 8(c), respectively. The compound nuclei formed via the even-A projectiles are more likely to de-excite through neutron emission, due to their relatively higher $B_{\rm f}$ values and lower $B_{\rm n}$ values, This behavior results in the odd-even staggering in both the survival probabilities and the maximal ERCSs of the Ti-induced reactions. Furthermore, the combined effect of the $B_{\rm n}$ and $B_{\rm f}$ values contributes to the generally higher survival probabilities in the reactions with the ^{254}Es target compared to those with ^{252}Es target. This dual enhancement in both the fusion and survival stages highlights the advantage of employing the ^{254}Es target for the synthesis of the isotopes with Z = 121.

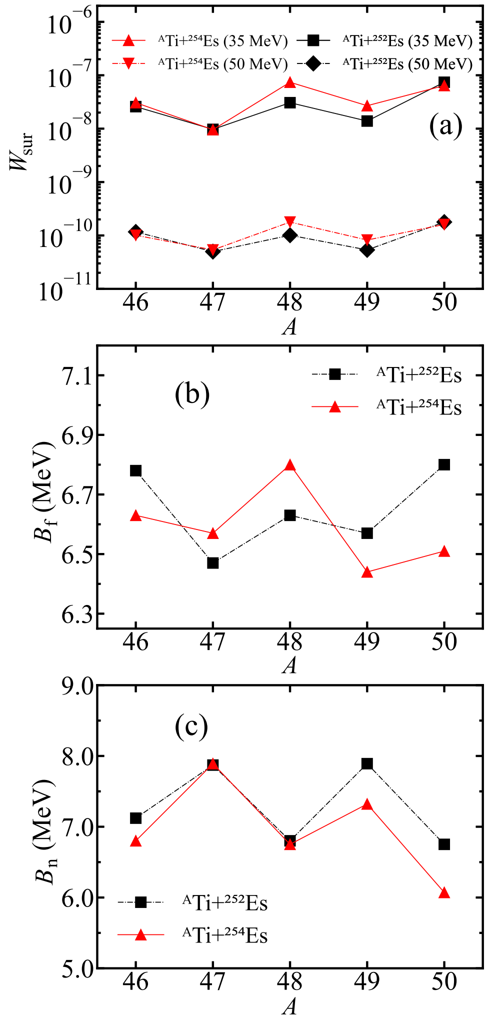

Fig. 8. (Color online) (a) The calculated survival probabilities of compound nuclei in the 3n-emission channel for the reactions $^{46-50}$Ti+^{252}Es and $^{46-50}$Ti+^{254}Es with $E^*_{\rm CN}$ = 35 MeV and $E^*_{\rm CN}$ = 50 MeV. (b) The $B_{\rm f}$ values and (c) the $B_{\rm n}$ values of the corresponding compound nuclei.

IV. SUMMARY

The calculated ERCSs using the DNS model are assessed with experimental results of the reactions ^{48}Ca + ^{245}Cm, ^{48}Ca + ^{248}Cm, ^{48}Ca + ^{249}Bk, and ^{48}Ca + ^{249}Cf. Our analysis indicates consistency between the theoretical predictions and experimental results. Based on the DNS model, we investigated the synthesis of SHE $Z = 121$ employing stable projectiles with $Z = 21 - 30$ and actinide targets with half-lives longer than 50 days, revealing that this element is expected to be produced via the reactions ^{45}Sc+^{257}Fm, ^{46}Ti + ^{254}Es and ^{46}Ti + ^{252}Es. Considering experimental feasibility, the reactions ^{46}Ti + ^{254}Es and ^{46}Ti + ^{252}Es are more favorable with the maximal ERCSs and optimal incident energies of 6.619 fb at 219.9 MeV and 4.123 fb at 223.9 MeV.

We investigate the mass asymmetry effect, revealing the

enhanced fusion probabilities for the Sc and Ti-induced reactions. Additionally, the influence of the Q values, the Coulomb barriers, the inner fusion barriers, the fission barriers and the neutron separation energies on the isotopic dependence of reactions with Ti projectiles and Es targets are analyzed in detail. Our results indicate that the employment of the ^{254}Es target and the even-A Ti projectiles with smaller neutron excess is favorable for synthesizing the element Z = 121.

---

[1] A. Sobiczewski, F. A. Gareev, B. N. Kalinkin, Closed shells for $Z > 82$ and $N > 126$ in a diffuse potential well. Phys. Lett **22**. 500–502 (1966). doi:10.1016/0031-9163(66)91243-1

[2] P. Möller, J. R. Nix, Stability of heavy and superheavy elements. J. Phys. G: Nucl. Part. Phys **20**, 1681–1747 (1994). doi:10.1088/0954-3899/20/11/003

[3] S. Ćwiok, P.-H. Heenen, W. Nazarewicz, Shape coexistence and triaxiality in the superheavy nuclei. Nature **433**, 705–709 (2005). doi:10.1038/nature03336

[4] S. Hofmann, G. Münzenberg, The discovery of the heaviest elements. Rev. Mod. Phys. **72**, 733–767 (2000). doi:10.1103/RevModPhys.72.733

[5] K. Morita, K. Morimoto, D. Kaji et al., Experiment on the synthesis of element 113 in the reaction ^{209}Bi (^{70}Zn, n) ^{278}113. J. Phys. Soc. Jpn **73**, 2593–2596 (2004). doi:10.1143/jpsj.73.2593

[6] Y. T. Oganessian, V. K. Utyonkov, Y. V. Lobanov et al., Attempt to produce element 120 in the ^{244}Pu+ ^{58}Fe reaction. Phys. Rev. C **79**, 024603 (2009). doi:10.1103/PhysRevC.79.024603

[7] Y. T. Oganessian, V. K. Utyonkov, Super-heavy element research. Rep. Prog. Phys **78**, 036301 (2015). doi:10.1088/0034-4885/78/3/036301

[8] Y. T. Oganessian, A. V. Yeremin, A. G. Popeko et al., Synthesis of nuclei of the superheavy element 114 in reactions induced by ^{48}Ca. Nature **400**, 242–245 (1999). doi:doi.org/10.1038/22281

[9] Y. T. Oganessian, F. S. Abdullin, S. N. Dmitriev et al., Investigation of the ^{243}Am+ ^{48} Ca reaction products previously observed in the experiments on elements 113, 115, and 117. Phys. Rev. C **87**, 014302 (2013). doi:10.1103/PhysRevC.87.014302

[10] Y. T. Oganessian, V. K. Utyonkov, Y. V. Lobanov, et al., Observation of the decay of ^{292}116. Phys. Rev. C **63**, 011301(R) (2000). doi:10.1103/PhysRevC.63.011301

[11] Y. T. Oganessian, F. S. Abdullin, P. D. Bailey et al., Synthesis of a new element with atomic number Z = 117. Phys. Rev. Lett **104**, 142502 (2010). doi:10.1103/PhysRevLett.104.142502

[12] Y. T. Oganessian, V. K. Utyonkov, Y. V. Lobanov et al., Synthesis of the isotopes of elements 118 and 116 in the ^{249}Cf and ^{245}Cm+ ^{48}Ca fusion reactions. Phys. Rev. C **74**, 044602 (2006). doi:10.1103/PhysRevC.74.044602

[13] S. Hofmann, Synthesis of superheavy elements by cold fusion. Radiochim. Acta **99**, 405–428 (2011). doi:10.1524/ract.2011.1854

[14] A. V. Yeremin, Regularities of formation and survival probability of compound nuclei in the region of $Z \geq 82$: study of complete-fusion reactions with heavy ions using the kinematic separator VASSILISSA. Phys. Part. Nucl **38**, 492–524 (2007). doi:10.1134/S1063779607040041

[15] Z. Y. Zhang, Z. G. Gan, L. Ma et al., Observation of the Superheavy Nuclide ^{271}Ds. Chin. Phys. Lett **29**, 012502 (2012). doi:10.1088/0256-307X/29/1/012502

[16] Y. T. Oganessian, V. K. Utyonkov, N. D. Kovrizhnykh et al., New isotope ^{286}Mc produced in the ^{243}Am+^{48}Ca reaction. Phys. Rev. C **106**, 064306 (2022). doi:10.1103/PhysRevC.106.064306

[17] S. Hofmann, S. Heinz, R. Mann et al., Review of even element super-heavy nuclei and search for element 120. Eur. Phys. J. A **52**, 180–213 (2016). doi:10.1140/epja/i2016-16180-4

[18] F. Heßberger, D. Ackermann, Some critical remarks on a sequence of events interpreted to possibly originate from a decay chain of an element 120 isotope. Eur. Phys. J. A **53**, 123–131 (2017). doi:10.1140/epja/i2017-12307-5

[19] J. Khuyagbaatar, A. Yakushev, C. E. Düllmann et al., Search for elements 119 and 120. Phys. Rev. C **102**, 064602 (2020). doi:10.1103/PhysRevC.102.064602

[20] M. Tanaka, P. Brionnet, M. Du et al., Probing optimal reaction energy for synthesis of element 119 from ^{51}V+^{248}Cm reaction with quasielastic barrier distribution measurement. J. Phys. Soc. Jpn **91**, 084201 (2022). doi:10.7566/JPSJ.91.084201

[21] Y. H. Zhang, G. Zhang, J. J. Li et al., Production cross sections of $^{243-248}$No isotopes in fusion reactions. Phys. Rev. C **106**, 014625 (2022). doi:10.1103/PhysRevC.106.014625

[22] K. Sekizawa, K. Hagino, Time-dependent Hartree-Fock plus Langevin approach for hot fusion reactions to synthesize the Z=120 superheavy element. Phys. Rev. C **99**, 051602(R) (2019). doi:10.1103/PhysRevC.99.051602

[23] L. Li, L. Guo, K. Godbey et al., Impact of tensor force on quantum shell effects in quasifission reactions. Phys. Lett. B **833**, 137349 (2022). doi:10.1016/j.physletb.2022.137349

[24] X. X. Sun, L. Guo, Microscopic study of fusion reactions with a weakly bound nucleus: Effects of deformed halo. Phys. Rev. C **107**, L011601 (2023). doi:10.1103/PhysRevC.107.L011601

[25] X. X. Sun, L. Guo, Microscopic study of the hot-fusion reaction ^{48}Ca +^{238} U with the constraints from time-dependent Hartree-Fock theory. Phys. Rev. C **107**, 064609 (2023). doi:10.1103/PhysRevC.107.064609

[26] T. Cap, M. Kowal, K. Siwek-Wilczynska, The Fusion-by-Diffusion model as a tool to calculate cross sections for the production of superheavy nuclei. Eur. Phys. J. A **58**, 231–248 (2022). doi:10.1140/epja/s10050-022-00891-8

[27] S. Chopra, M. K. Sharma, P. O. Hess et al., Possibility to form Z=120 via the ^{64}Ni+^{238}U reaction using the dynamical cluster-decay model. Phys. Rev. C **105**, 014610 (2022). doi:10.1103/PhysRevC.105.014610

[28] D. Boilley, Y. Abe, B. Cauchois et al., Elimination of fast variables and initial slip: a new mechanism for fusion hindrance in heavy-ion collisions. J. Phys. G: Nucl. Part. Phys **46**, 115102 (2019) . doi:10.1088/1361-6471/ab11ef

[29] L. Liu, C. W. Shen, Q. F. Li et al., Residue cross sections of ^{50}Ti-induced fusion reactions based on the two-step model. Eur. Phys. J. A **52**, 35–39 (2016). doi:10.1140/epja/i2016-16035-0

[30] G. G. Adamian, N. V. Antonenko, W. Scheid et al., Fusion cross sections for superheavy nuclei in the dinuclear system concept. Nucl. Phys. A **633**, 409–420 (1998). doi:10.1016/S0375-9474(98)00124-9

[31] G. Zhang, C. A. T. Sokhna, Z. Liu et al., Production of neutron-rich isotopes ^{264,266,268,269}Rf by multinucleon transfer reac-

tions based on ^{238}U beam. Phys. Rev. C **100**, 024613 (2019). doi:10.1103/PhysRevC.100.024613
[32] L. Zhu, J. Su, F. S. Zhang, Influence of the neutron numbers of projectile and target on the evaporation residue cross sections in hot fusion reactions. Phys. Rev. C **93**, 064610 (2016). doi:10.1103/PhysRevC.93.064610
[33] F. Li, L. Zhu, Z. H. Wu et al., Predictions for the synthesis of superheavy elements Z = 119 and 120. Phys. Rev. C **98**, 014618 (2018). doi:10.1103/PhysRevC.98.014618
[34] P. W. Wen, A. K. Nasirov, C. J. Lin et al., Multinucleon transfer reaction from view point of dynamical dinuclear system method. J. Phys. G: Nucl. Part. Phys **47**, 075106 (2020). doi:10.1088/1361-6471/ab8dcc
[35] N. Wang, E. G. Zhao, W. Scheid et al., Theoretical study of the synthesis of superheavy nuclei with Z=119 and 120 in heavy-ion reactions with trans-uranium targets. Phys. Rev. C **85**, 041601(R) (2012). doi:10.1103/PhysRevC.85.041601
[36] X. J. Bao, S. Q. Guo, H. F. Zhang et al., Influence of entrance channel on production cross sections of superheavy nuclei. Phys. Rev. C **96**, 024610 (2017). doi:10.1103/PhysRevC.85.041601
[37] X. B. Yu, L. Zhu, Z. H. Wu et al., Predictions for production of superheavy nuclei with z = 105-112 in hot fusion reactions. Nucl. Sci. Tech **29**, 154 (2018). doi:10.1007/s41365-018-0501-2
[38] P. H. Chen, H. Wu, Z. X. Yang et al., Prediction of synthesis cross sections of new moscovium isotopes in fusion-evaporation reactions. Nucl. Sci. Tech **34**, 7 (2023). doi:10.1007/s41365-022-01157-0
[39] C. Li, P. W. Wen, J. J. Li et al., Production of heavy neutron-rich nuclei with radioactive beams in multinucleon transfer reactions. Nucl. Sci. Tech **28**, 110 (2017). doi:10.1007/s41365-017-0266-z
[40] M. T. Jin, S. Y. Xu, G. M. Yang et al., Yield of long-lived fission product transmutation using proton-, deuteron-, and alpha particle-induced spallation. Nucl. Sci. Tech **32**, 96 (2021). doi:10.1007/s41365-021-00933-8
[41] M. H. Zhang, Y. H. Zhang, Y. Zou, C. Wang, L. Zhu, F. S. Zhang, Predictions of synthesizing elements with Z = 119 and 120 in fusion reactions, Phys. Rev. C **109** 014622 (2024). doi:10.1103/PhysRevC.109.014622.
[42] P. H. Chen, C. Geng, Z. X. Yang, X. H. Zeng, Z. Q. Feng, Production of neutron-rich actinide isotopes in isobaric collisions via multinucleon transfer reactions, Nucl. Sci. Tech **34** 160 (2023). doi:10.1007/s41365-023-01314-z.
[43] S. Y. Xu, Z. Q. Feng, Cluster emission in massive transfer reactions based on dinuclear system model, Nucl. Tech **46**, 030501 (2023). doi:10.11889/j.0253-3219.2023.hjs.46.030501.
[44] M. H. Zhang, Y. H. Zhang, J. J. Li, N. Tang, S. Sun, F. S. Zhang, Progress in transport models of heavy-ion collisions for the synthesis of superheavy nuclei, Nucl. Tech **46**, 137 (2023). doi:10.11889/j.0253-3219.2023.hjs.46.080014
[45] L. Zhu, W. J. Xie, F. S. Zhang, Production cross sections of superheavy elements Z = 119 and 120 in hot fusion reactions, Phys. Rev. C **89**, 024615 (2014). doi:10.1103/PhysRevC.89.024615
[46] X. J. Lv, Z. Y. Yue, W. J. Zhao et al., Theoretical study of evaporation-residue cross sections of superheavy nuclei. Phys. Rev. C **103**, 064616 (2021). doi:10.1103/PhysRevC.103.064616
[47] N. Wang, J. L. Tian, W. Scheid, Systematics of fusion probability in ''hot'' fusion reactions. Phys. Rev. C **84**, 061601(R) (2011). doi:10.1103/PhysRevC.84.061601
[48] N. Wang, X. Wu, Z. Li et al., Applications of skyrme energy-density functional to fusion reactions for synthesis of superheavy nuclei. Phys. Rev. C **74**, 044604 (2006). doi:10.1103/PhysRevC.74.044604
[49] X. J. Bao, Possibilities for synthesis of new neutron-deficient isotopes of superheavy nuclei*. Chin. Phys. C **43**, 054105 (2019). doi:10.1088/1674-1137/43/5/054105
[50] J. X. Li, H. F. Zhang, Predictions for the synthesis of the Z=120 superheavy element. Phys. Rev. C **106**, 034613 (2022). doi:10.1103/PhysRevC.106.034613
[51] X. Q. Deng, S. G. Zhou, Examination of promising reactions with ^{241}Am and ^{244}Cm targets for the synthesis of new superheavy elements within the dinuclear system model with a dynamical potential energy surface. Phys. Rev. C **107**, 014616 (2023). doi:10.1103/PhysRevC.107.014616
[52] B. M. Kayumov, O. K. Ganiev, A. K. Nasirov et al., Analysis of the fusion mechanism in the synthesis of superheavy element 119 via the ^{54}Cr+^{243}Am reaction. Phys. Rev. C **105**, 014618 (2022). doi:10.1103/PhysRevC.105.014618
[53] J. Hong, G. G. Adamian, N. V. Antonenko et al., Hot and cold fusion reactions leading to the same superheavy evaporation residue. Eur. Phys. J. A **58**, 180–183 (2022). doi:10.1140/epja/s10050-022-00826-3
[54] K. X. Cheng, J. Pu, Y. T. Wang et al., Non-frozen process of heavy-ion fusion reactions at deep sub-barrier energies, Nucl. Sci. Tech **33**, 132 (2022). doi:10.1007/s41365-022-01114-x
[55] B. Li, N. Tang, Y. H. Zhang et al., Production of p-rich nuclei with z= 20-25 based on radioactive ion beams. Nucl. Sci. Tech **33**, 55 (2022). doi:10.1007/s41365-022-01048-4
[56] T. P. Luo, P. W. Wen, C. J. Lin et al., Bayesian analysis on non-resonant behavior of ^{12}C + ^{12}C fusion reaction at sub-barrier energies. Chin. Phys. C **46**, 064105 (2022). doi:10.1088/1674-1137/ac5587
[57] S. H. Zhu, X. J. Bao, Possibility to synthesize $Z = 120$ superheavy nuclei with $Z > 20$ projectiles. Phys. Rev. C **108**, 014604 (2023). doi:10.1103/PhysRevC.108.014604
[58] B. S. Cai, C. X. Yuan, Random forest-based prediction of decay modes and half-lives of superheavy nuclei, Nucl. Sci. Tech **34** 204 (2023). doi:10.1007/s41365-023-01354-5
[59] Z. Wang, Z. Z. Ren, Predictions of the decay properties of the superheavy nuclei ^{293,294}119 and ^{294,295}120, Nucl. Tech **46** 114 (2023). doi:10.11889/j.0253-3219.2023.hjs.46.080011
[60] V. I. Zagrebaev, Synthesis of superheavy nuclei: Nucleon collectivization as a mechanism for compound nucleus formation. Phys. Rev. C **64**, 034606 (2001). doi:10.1103/PhysRevC.64.034606
[61] A. S. Zubov, G. G. Adamian, N. V. Antonenko et al., Survival probability of superheavy nuclei. Phys. Rev. C **65**, 024308 (2002). doi:10.1103/PhysRevC.65.024308
[62] Z. Q. Feng, G. M. Jin, F. Fu et al., Production cross sections of superheavy nuclei based on dinuclear system model. Nucl. Phys. A **771**, 50–67 (2006). doi:10.1016/j.nuclphysa.2006.03.002
[63] W. D. Myers, W. J. Swiatecki, Nuclear masses and deformations. Nuclear Physics **81**, 1–60 (1966). doi:10.1016/0029-5582(66)90639-0
[64] C. Y. Wong, Interaction barrier in charged-particle nuclear reactions. Phys. Rev. Lett. **31**, 766–769 (1973). doi:10.1103/PhysRevLett.31.766
[65] Z. Ahmed, Tunnelling through the morse barrier. Phys. Lett. A **157**, 1–5 (1991). doi:10.1016/0375-9601(91)90399-S
[66] V. Y. Denisov, Expression for the heavy-ion fusion cross section. Phys. Rev. C **107**, 054618 (2023).

doi:10.1103/PhysRevC.107.054618

[67] S. Rana, R. Kumar, S. Patra et al., Fusion dynamics of astrophysical reactions using different transmission coefficients. Eur. Phys. J. A **58**, 241 (2022). doi:10.1140/epja/s10050-022-00893-6

[68] B. Wang, K. Wen, W. J. Zhao et al., Systematics of capture and fusion dynamics in heavy-ion collisions. At. Data Nucl. Data Tables **114**, 281–370 (2017). doi:10.1016/j.adt.2016.06.003

[69] P. Möller, A. Sierk, T. Ichikawa et al., Nuclear ground-state masses and deformations: FRDM(2012). At. Data. Nucl. Data Tables. **109-110**, 1–204 (2016). doi:doi.org/10.1016/j.adt.2015.10.002

[70] N. Wang, L. Dou, E. G. Zhao et al., Nuclear hexadecapole deformation effects on the production of super-heavy elements. Chin. Phys. Lett. **27**, 062502 (2010). doi:10.1088/0256-307X/27/6/062502

[71] J. Q. Li, G. Wolschin, Distribution of the dissipated angular momentum in heavy-ion collisions. Phys. Rev. C **27**, 590–601 (1983). doi:10.1103/PhysRevC.27.590

[72] S. Ayik, B. Schürmann, W. Nörenberg, Microscopic transport theory of heavy-ion collisions. Z. Phys. A **277**, 299–310 (1976). doi:10.1007/BF01415605

[73] G. G. Adamian, N. V. Antonenko, W. Scheid, Characteristics of quasifission products within the dinuclear system model. Phys. Rev. C **68**, 034601 (2003). doi:10.1103/PhysRevC.68.034601

[74] X. J. Bao, Y. Gao, J. Q. Li et al., Influence of the nuclear dynamical deformation on production cross sections of superheavy nuclei. Phys. Rev. C **91**, 011603 (2015). doi:10.1103/PhysRevC.91.011603

[75] J. D. Jackson, A schematic model for (p, xn) cross sections in heavy elements. Can. J. Phys. **34**, 767–779 (1956). doi:10.1139/p56-087

[76] V. Weisskopf, Statistics and Nuclear Reactions. Phys. Rev. **52**, 295–303 (1937). doi:10.1103/PhysRev.52.295

[77] A. V. Ignatyuk, K. K. Istekov, G. N. Smirenkin, Role of the collective effects in a systematics of nuclear level density. Sov. J. Nucl. Phys. **29**, 875 (1979).

[78] M. Blann, Decay of deformed and superdeformed nuclei formed in heavy ion reactions. Phys. Rev. C **21**, 1770–1782 (1980). doi:10.1103/PhysRevC.21.1770

[79] N. Bohr, J. A. Wheeler, The mechanism of nuclear fission. Phys. Rev. **56**, 426–450 (1939). doi:10.1103/PhysRev.56.426

[80] G. G. Adamian, N. V. Antonenko, S. P. Ivanova et al., Analysis of survival probability of superheavy nuclei. Phys. Rev. C **62**, 064303 (2000). doi:10.1103/PhysRevC.62.064303

[81] A. S. Zubov, G. G. Adamian, N. V. Antonenko et al., Survival probabilities of superheavy nuclei based on recent predictions of nuclear properties. Eur. Phys. J. A **23**, 249 (2005). doi:10.1140/epja/i2004-10089-5

[82] L. Zhu, Selection of projectiles for producing trans-uranium nuclei in transfer reactions within the improved dinuclear system model. J. Phys. G: Nucl. Part. Phys **47**, 065107 (2020). doi:10.1088/1361-6471/ab871f

[83] V. Y. Denisov, I. Y. Sedykh, Calculation of the fission width of an excited nucleus with the fission barrier dependent on excitation energy. Phys. Rev. C **98**, 024601 (2018). doi:10.1103/PhysRevC.98.024601

[84] W. F. Li, Z. Z. Wang, H. S. Xu et al., Odd–Even Effects of the Survival Probability for Superheavy Compound Nuclei. Chin. Phys. Lett. **21**, 636 (2004). doi:10.1088/0256-307X/21/4/013

[85] C. J. Xia, B. X. Sun, E. G. Zhao et al., Systematic study of survival probability of excited superheavy nuclei. Sci. China Phys. Mech. Astron. **54**, 109–113 (2011). doi:10.1007/s11433-011-4438-2

[86] Y. T. Oganessian, V. K. Utyonkov, Y. V. Lobanov et al., Measurements of cross sections for the fusion-evaporation reactions ^{244}Pu (^{48}Ca, xn) $^{292-x}$114 and ^{245}Cm (^{48}Ca, xn) $^{293-x}$116. Phys. Rev. C **69**, 054607 (2004). doi:10.1103/PhysRevC.69.054607

[87] Y. T. Oganessian, V. K. Utyonkov, Y. V. Lobanov et al., Measurements of cross sections and decay properties of the isotopes of elements 112, 114, and 116 produced in the fusion reactions ^{233,238}U, ^{242}Pu, and ^{248}Cm+^{48}Ca. Phys. Rev. C **70**, 064609 (2004). doi:10.1103/PhysRevC.70.064609

[88] Y. T. Oganessian, F. S. Abdullin, C. Alexander et al., Studies of the ^{249}Bk+ ^{48}Ca reaction including decay properties and excitation function for isotopes of element 117 and discovery of the new isotope ^{277}Mt. Phys. Rev. C **87**, 054621 (2013). doi:10.1103/PhysRevC.87.054621

[89] Y. T. Oganessian, F. S. Abdullin, C. Alexander et al., Production and decay of the heaviest nuclei ^{293,294}117 and ^{294}118. Phys. Rev. Lett **109**, 162501 (2012). doi:10.1103/PhysRevLett.109.162501

[90] A. A. Voinov, Y. T. Oganessian, F. S. Abdullin et al., Study of the $^{249-251}$Cf+ ^{48}Ca reactions: recent results and outlook. J. Phys: Conf. Ser **966**, 012057 (2018). doi:10.1088/1742-6596/966/1/012057

[91] H. Lü, D. Boilley, Y. Abe et al., Synthesis of superheavy elements: Uncertainty analysis to improve the predictive power of reaction models. Phys. Rev. C **94**, 034616 (2016). doi:10.1103/PhysRevC.94.034616

[92] J. A. Sheikh, W. Nazarewicz, J. C. Pei, Systematic study of fission barriers of excited superheavy nuclei. Phys. Rev. C **80**, 011302(R) (2009). doi:10.1103/PhysRevC.80.011302

[93] F. G. Kondev, M. Wang, W. J. Huang et al., The NUBASE2020 evaluation of nuclear physics properties. Chin. Phys. C **45**, 030001 (2021). doi:10.1088/1674-1137/abddae

[94] R. W. Lougheed, J. H. Landrum, E. K. Hulet et al., Search for superheavy elements using the ^{48}Ca+^{254}Es^{g} reaction. Phys. Rev. C **32**, 1760–1763 (1985). doi:10.1103/PhysRevC.32.1760